

Design and performance of a stable linear retarder

K. B. Rochford, A. H. Rose, P. A. Williams, C. M. Wang, I. G. Clarke, P. D. Hale, and G. W. Day

The National Institute of Standards and Technology (NIST) has developed a nominally quarter-wave linear retarder for wavelengths near $1.3\ \mu\text{m}$ that is stable within $\pm 0.1^\circ$ retardance over a range of wavelength, input angle, temperature, and environmental variations. The device consists of two concatenated Fresnel rhombs made from a low stress-optic-coefficient glass that minimizes the residual birefringence from machining and packaging. Device machining, assembly, and antireflection coating tolerances are discussed, and the theoretical performance is compared with measurements. Humidity can modify retardance of the total-internal-reflection surfaces; we discuss packaging that mitigates this effect and provides an estimated 10-year lifetime for the device. Several measurement methods were intercompared to ensure that the device retardance can be measured with an uncertainty less than 0.1° . Similar retarders will be certified by NIST and made available as Standard Reference Materials.

Key words: Polarization, retarder, retardance measurement, standards, wave plate.

1. Introduction

We review the design, fabrication, and characterization of a stable linear retarder. After listing performance objectives, we examine the theoretical performance of our device and describe the fabrication and the assembly tolerances. Packaging issues related to environmental stability are discussed, and we provide estimates of the useful life of the device. Three methods used to measure retardance are described and measurements of five stable retarders are presented. Finally, data showing variation of retardance for several operational parameters are presented.

Our goal was to fabricate and to characterize a nominally quarter-wave retarder for use at $\lambda = 1.3 \pm 0.05\ \mu\text{m}$, with the exact retardance known within 0.1° . Ideally, the device would have $\pm 0.1^\circ$ retardance stability for practical variations in wavelength, input angle, and temperature, and have collinear in-

put and output beams. Because birefringent retarders typically exhibit significant wavelength dependence,¹ we focused our efforts on total-internal-reflection (TIR) devices such as Fresnel rhombs.²

2. Double-Rhomb Retarder

Earlier theoretical evaluations of TIR retarders show that these devices are nearly achromatic and can be tolerant of input angle deviations.³⁻⁶ In practice, however, TIR devices rarely achieve their theoretical performance because the stress-induced birefringence that occurs during the production, machining, or polishing of glass introduces a spatially varying retardance throughout the device. Recognizing this, researchers suggested that rhomb designs with short optical paths (and with the least retardance owing to birefringence) are superior to longer-path designs.^{3,7} This suggests that a double-rhomb design^{8,9} (see Fig. 1) is unsatisfactory despite the excellent performance (including the greatest tolerance to input-angle variations) it otherwise exhibits.^{3,7}

To overcome the limitations arising from glass birefringence, we examined TIR retarders made from a lead-doped flint glass (glass code 847238) (see Ref. 10) that has a remarkably low stress-optic coefficient. The stress-optic coefficient is 0 at a wavelength near 570 nm and is 1 order of magnitude lower than that of other glasses throughout the visible.¹¹ Though it is more difficult to polish than the borosilicate glasses or the fused silica often used for rhombs, complex

K. B. Rochford, A. H. Rose, P. A. Williams, C. M. Wang, P. D. Hale, and G. W. Day are with the National Institute of Standards and Technology, 325 Broadway Street, Boulder, Colorado 80303-3328. K. B. Rochford, A. H. Rose, P. A. Williams, P. D. Hale, and G. W. Day are in the Optoelectronics Division and C. W. Wang is in the Statistical Engineering Division. I. G. Clarke is now with Galileo Corporation, Galileo Park, P.O. Box 550, Sturbridge, Massachusetts 01566.

Received 8 October 1996; revised manuscript received 5 February 1997.

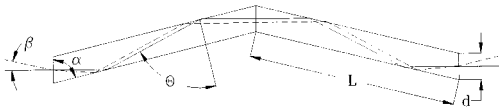


Fig. 1. Schematic of double-rhomb retarder; for our device $d = 10$ mm, $\alpha \approx 76.4^\circ$, and $L \approx 80$ mm.

structures made from this glass have been successfully used for optical current sensing, another application that requires very low birefringence.¹² Our measurements of blocks of this glass showed negligible retardance over most of the cross section and significant retardance only within 0.5 mm of the machined edges.² We used this material to fabricate the double-rhomb Fresnel retarders described in this paper.

3. Theoretical Performance

Four reflections with 22.5° retardance are necessary to obtain a quarter-wave TIR retarder with the double rhomb. Sellmeier equations for the flint glass yield a refractive index $n = 1.8055$ at $1.32 \mu\text{m}$ (see Ref. 13). The retardance imparted by a reflection at angle θ , calculated from Fresnel's equation,¹⁴ is

$$\Gamma(\theta) = 2 \tan^{-1} \left[\frac{\cos \theta (\sin^2 \theta - (1/n)^2)^{1/2}}{\sin^2 \theta} \right], \quad (1)$$

and, as shown in Fig. 2, equals 22.5° for two angles of incidence.

Figure 1 shows that the pairs of reflections are complementary; an increase in the first two TIR angles (due to nonnormal incidence) leads to a decrease in the last two angles. Thus if retardance varies linearly with the TIR angle, the retardance changes cancel, and a wider range of incidence angle variation can be tolerated. A compact, shorter-path-length device can be made if the rhombs are cut so that the lower incidence angle is used. However, we selected the larger TIR angle $\theta_0 = 76.39^\circ$ because the relative linearity of the retardance variation about this angle allows a larger input-angle range.

A. Retardance Error Due to Input Angle Variation

Rhomb cut with $\alpha = \theta_0$ provide 22.5° retardance at each reflection. When light is incident at an angle β

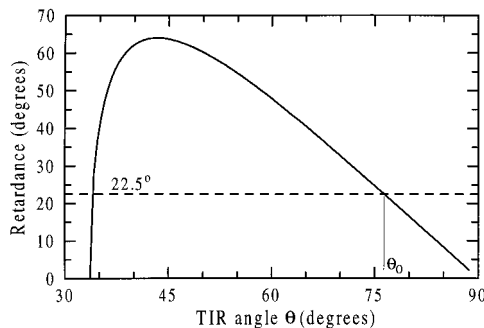


Fig. 2. TIR angle dependence of retardance for glass with $n = 1.8055$.

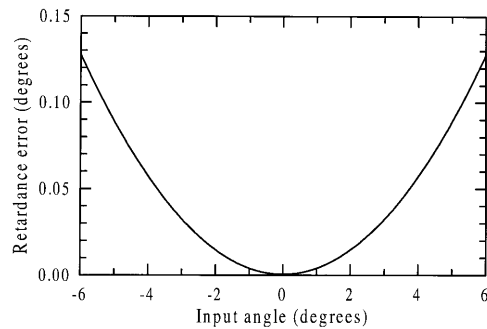


Fig. 3. Theoretical plot of retardance for various input angles.

with respect to the entrance face normal (see Fig. 1), application of Snell's law shows that the TIR angles change by $\pm \sin^{-1}(\sin \beta / n)$. The retardance error $\Delta \delta_\beta$ resulting from input-angle variation is

$$\Delta \delta_\beta = 4\Gamma(\alpha) - 2\Gamma[\alpha + \sin^{-1}(\sin \beta / n)] - 2\Gamma[\alpha - \sin^{-1}(\sin \beta / n)] \quad (2)$$

and is plotted in Fig. 3. Input-angle variation decreases retardance, and limiting this decrease to 0.1° restricts the allowed misalignment β to $\pm 5.3^\circ$, which we easily realized by monitoring backreflection. By ray tracing, however, we find that β must be limited to $\pm 1.8^\circ$ to ensure that all input rays undergo exactly four reflections and exit parallel to the input. Thus by monitoring the transmission of a fully illuminated input face, we can hold misalignment well below the $\pm 5.3^\circ$ for which the retardance decrease is within 0.1° .

B. Retardance Error Due to Wavelength Variation

We estimate the wavelength dependence of retardance using the Sellmeier equation. Figure 4 shows that the retardance is within $90^\circ \pm 0.1^\circ$ from 1130 to 1560 nm. Over the internal transmission range of the glass (see Fig. 5), the retardance is nominally quarter wave and varies from 89.6° to 92.4° . In principle, this design can serve as a stable retarder for any wavelength between 400 and 2200 nm if one simply characterizes performance at the target wavelength.

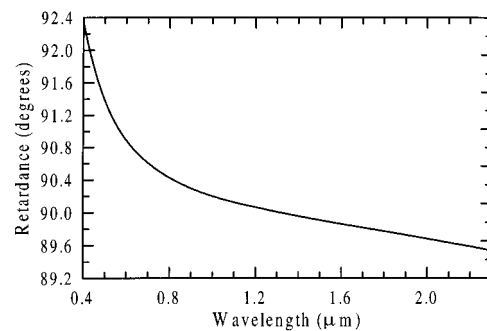


Fig. 4. Wavelength dependence of retardance calculated from Sellmeier equation.

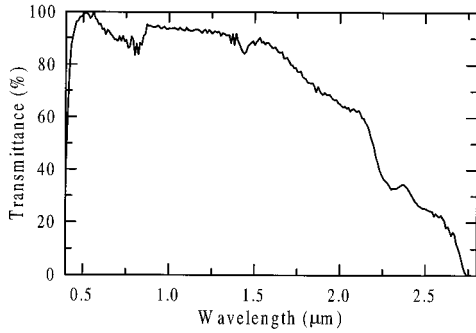


Fig. 5. Transmission spectrum of a double-rhomb retarder.

C. Retardance Error Due to Coherent Reflections

In practice, the wavelength range that offers $\pm 0.1^\circ$ retardance stability may be limited by the bandwidth of antireflection coatings applied to the entrance, exit, and internal faces of the double rhomb. Coatings are essential when coherent light is used because interfacial reflections lead to multiple passes through the retarder that can interfere with and modify the retardance.

For a perfectly coherent source, the change in retardance resulting from reflections $\Delta\delta(R)$ can be found by summing the individual fields that contribute to the transmitted fields.¹⁵ For reflectance R ,

$$\Delta\delta[R, \phi(t)] = \tan^{-1} \left\{ \frac{R \sin[\phi(t) - \delta_0]}{1 - R \cos[\phi(t) - \delta_0]} \right\} - \tan^{-1} \left\{ \frac{R \sin[\phi(t) + \delta_0]}{1 - R \cos[\phi(t) + \delta_0]} \right\}, \quad (3)$$

where δ_0 is the device TIR retardance, and the round-trip phase $\phi(t)$ typically varies with time as temperature fluctuations change the optical path length of the rhomb. Assuming that $\phi(t)$ is a uniformly distributed random variable over $[0, 2\pi]$, the probability density function for $\Delta\delta(R)$ is¹⁶

$$P(\Delta\delta) = \frac{(1 - R^2) \sin(\delta_0)}{\pi |\sin(\delta_0 - \Delta\delta)| \{4R^2 \sin^2(\delta_0 - \Delta\delta) - [\sin(\Delta\delta) - R^2 \sin(2\delta_0 - \Delta\delta)]^2\}^{1/2}}, \quad (4)$$

for

$$\tan^{-1} \left[\frac{R^2 \sin(2\delta_0) - 2R \sin(\delta_0)}{1 + R^2 \cos(2\delta_0) - 2R \cos(\delta_0)} \right] < \Delta\delta < \tan^{-1} \left[\frac{R^2 \sin(2\delta_0) + 2R \sin(\delta_0)}{1 + R^2 \cos(2\delta_0) + 2R \cos(\delta_0)} \right].$$

$P(\Delta\delta)$ is a U-shaped distribution with maximum errors given by the extrema of $\Delta\delta$ in Eq. 4. The mean error is zero, however, and the average of repeated measurements over all values of $\phi(t)$ will yield δ_0 .

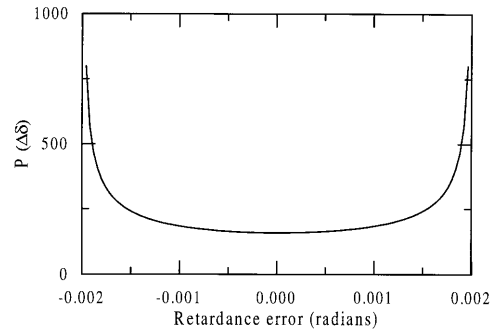


Fig. 6. Probability density function for retardance errors arising from coherent reflections in a 90° retarder. The probability that the retardance error is between δ_1 and δ_2 is found through integrating $P(\Delta\delta)$ from δ_1 to δ_2 .

Error is greatest for a rhomb with $\delta_0 = 90^\circ$, and the probability density function reduces to

$$P(\delta_0 = 90^\circ; \Delta\delta) = \frac{\sec^2 \Delta\delta}{\pi \kappa [1 - (\tan \Delta\delta / \kappa)^2]^{1/2}}, \quad -\tan^{-1}(\kappa) < \Delta\delta < \tan^{-1}(\kappa), \quad (5)$$

where $\kappa = 2R/(1 - R^2)$. This function is shown in Fig. 6. For $\delta_0 = 90^\circ$ the maximum retardance error is $\Delta\delta_{\max}(R) = \pm \tan^{-1}[2R/(1 - R^2)]$, and in the limit of small reflectance, the standard deviation $\approx \sqrt{2} R$.

Consider a double-rhomb retarder with reflectance R_1 at each external end face and a reflectance R_2 at each internal interface between the single rhombs. Multiple reflections between the internal interface and end faces and between the end faces can contribute to retardance error. Including these three interference paths yields retardance error

$$\Delta\delta_c = \Delta\delta[R_e, \phi_1(t)] + \Delta\delta[R_e, \phi_2(t)] + \Delta\delta[R_1, \phi_1(t) + \phi_2(t)],$$

where $R_e = (R_1 \times R_2)^{1/2}$, and the round-trip phase of single rhombs $\phi_1(t)$ and $\phi_2(t)$ are independent uniform random variables on $[0, 2\pi]$. The resulting probability density function is more complicated than for the single-rhomb case, but for $\delta_0 \approx 90^\circ$, the maximum error for coherent reflections is $\epsilon_R = 2\Delta\delta_{\max}(R_e) + \Delta\delta_{\max}(R_1)$, the mean error is zero, and the standard deviation of the probability density function is $\sigma_R \approx [2(R_1^2 + R_e^2)]^{1/2}$.

We specified antireflection coatings with $< 0.1\%$ reflectance over a 150-nm range for the input and the output end faces of the double rhomb. The internal interface has an antireflection coating with $< 0.05\%$

reflectance (matched to the adhesive) over a similar wavelength range. In practice, we have assembled devices with coating reflectances $<0.05\%$ (measured with a calibrated spectrophotometer) for all interfaces. For a highly coherent source, a maximum retardance error of $\epsilon_R = \pm 0.17^\circ$ can result from such coatings.

Many sources for polarimetric measurements have coherence lengths of less than the ≈ 60 -cm optical path round trip in the double-rhomb device. For our stable retarder, a temperature change of 0.3°C is sufficient to change the optical path by 2π . Thus averaging repeated measurements made over a time long enough to allow slight temperature changes yields the true retardance even if the interference is coherent.

D. Retardance Error Due to Twist

Our retarder is made by attaching two rhombs with retardance $\delta_0/2$. During the assembly it is possible to introduce a small rotation, or twist ϵ_t , between the rhombs. If $\epsilon_t = 0$, we can then find the polarization axes by rotating the device between crossed polarizers and finding a transmission null. When $\epsilon_t \neq 0$, however, the best null occurs when the polarizer and the analyzer are not crossed, but have an angle error $\Delta\theta_t$. Twist is related to this polarizer angle offset by

$$\Delta\theta_t = \epsilon_t \left[\frac{2 \cos(\delta_0/2) - \cos(\delta_0) - 1}{\cos(\delta_0) + 1} \right]. \quad (6)$$

For $\delta_0 = 90^\circ$, $\epsilon_t \approx 2.4\Delta\theta_t$. We have fabricated devices with ϵ_t between 0° and 0.8° .

A device with twist might have elliptical eigenpolarizations, and this can lead to measurement errors in systems that assume the device under test has linear eigenpolarizations. For example, if a measurement method requires the retarder axes to be located by the rotation of the device between crossed polarizers until a null occurs, the best null occurs at an angle $\epsilon_n = -\epsilon_t/2$ from the position of the null found if $\epsilon_t = 0$. The impact of such effects on measurement accuracy can often be evaluated if the twist angle is known.

4. Fabrication and Assembly Tolerances

Our rhombs have square end faces with sides $d = 10$ mm (see Fig. 1). The length L of a single rhomb is chosen so that only two TIR's occur for a beam input at normal incidence. Ensuring that all rays normally incident upon the input face exit after two reflections requires that

$$L = 2d \sin \alpha \tan \alpha. \quad (7)$$

Because $\alpha \approx 76.4^\circ$ for our quarter-wave device, $L \approx 80$ mm for $d = 10$ mm.

If the rhomb surfaces are not parallel, the output optical beam can be either deviated or displaced upon exit. The end faces of each single rhomb must be parallel within $\pm 0.003^\circ$, and the long TIR surfaces must be parallel to $\pm 0.001^\circ$ to ensure that a normally

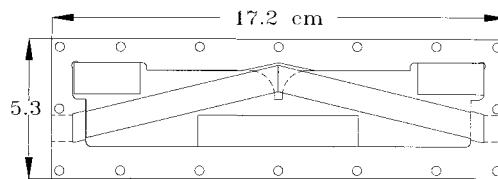


Fig. 7. Outline drawing of rhomb and protective packaging.

incident beam exits the double rhomb with less than $\pm 0.008^\circ$ deviation. (Small deviation is desired so the device can be used with optical-fiber-based polarimetric systems without excessive coupling loss.) For this machining tolerance, the output beam is displaced less than $\pm 6 \mu\text{m}$.

Assembling the double rhomb requires precision six-axis positioning (three translational and three angular degrees of freedom) to align the single-rhomb end faces, to minimize the wedge between the end faces, and to ensure that all TIR reflections lie within a plane. The wedge angle between the internal end faces is kept within $\pm 0.006^\circ$ to keep the beam deviation $<0.006^\circ$. Relative rotation or the out-of-plane twist between the rhombs should be less than 0.2° so that the principal retardance axis can be found within 0.1° . Rhomb rotation is aligned polarimetrically, and other alignments are optimized by the monitoring of the deflection of a normally incident He-Ne laser beam on a distant screen. After alignment, the single rhombs are joined together with a UV curing acrylate adhesive.

5. Packaging and Environmental Stability

Assembled rhombs are packaged in an aluminum housing (see Fig. 7) to protect them from contaminants that can interact with the TIR surface. The rhomb is attached to the base of the box at three points with a flexible epoxy. Epoxy is also used to fill and to seal the 0.5-mm gap between the sides of the rhomb end faces and the open optical access ports at the ends of the package. A Teflon gasket seals the lid to the box, and each assembly is leak tested to ensure integrity.

The glass is hygroscopic, and water vapor can adsorb onto the TIR surface and change retardance. To minimize changes, we designed the box to minimize water vapor transport into the interior cavity and to contain four vials of desiccant (molecular sieve) to maintain low humidity. We estimated retardance stability by measuring the effect of humidity on retardance and testing the effectiveness of our packaging.

We measured the retardance of an unpackaged double rhomb held at $\approx 26\%$ relative humidity (RH) and 25°C over 80 h. Assuming that retardance change resulting from humidity can be expressed as

$$\frac{d\Delta\delta(t)}{dt} = \Delta\delta_{RH}RH(t), \quad (8)$$

we find that $\Delta\delta_{RH} = 0.17 \pm 0.02^\circ/(\text{yr} \times \%RH)$ from six measurements. Extrapolation to long times

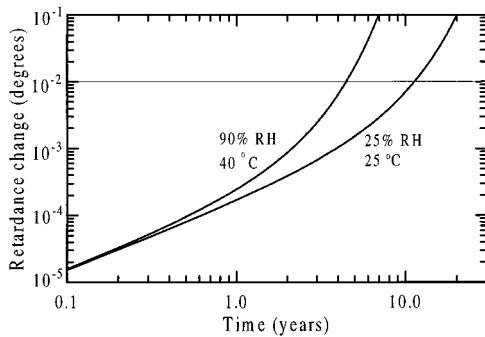


Fig. 8. Calculated change in retardance and internal humidity for two environmental conditions.

overestimates the change because the retardance saturates for long-term humidity exposure, but this allows us to estimate conservatively the humidity effects. Clearly, the interior humidity must remain below 0.01% to insure retardance stability of $<0.01^\circ$ over many years.

To estimate the interior humidity of our package, we calculated the water transport through the permeable seals. We confirmed our calculations by placing the package in a high-humidity environmental chamber and measuring the mass of water that leaked into the package. The calculated internal humidity was combined with the measured effect of humidity on retardance to determine the retardance stability of our device. We discuss this in greater detail in Appendix A.

Figure 8 shows the estimated retardance change $\Delta\delta(t)$ for packages exposed to two environments. A packaged rhomb exposed to 90% relative humidity at 40°C undergoes a retardance change of 0.01° in ≈ 4.5 yr. For 25% relative humidity at 25°C , ≈ 10 yr are needed to effect the same change.

6. Retardance Measurement Methods

We use three different methods to measure retardance so that accuracy can be demonstrated and studied. Two methods make use of modified versions of standard polarimetric measurements and require rotating polarizers. These are complemented by an interferometric method that is less sensitive to polarizer quality but is more sensitive to coherence effects in the retarders. We describe each method and report the expanded uncertainties U (which include a coverage factor of 2 so that the true value is within $\delta \pm U$ approximately 95% of the time¹⁷).

Our first method makes use of a standard polarimetric technique modified to reduce error sources.¹⁸ Linearly polarized light is incident upon the retarder, and the light emerges with an elliptical polarization. The intensities of the two orthogonal polarization states are measured simultaneously with a Wollaston polarizer and photodiodes. A governing equation relates the ratio of these two intensities to the orientations of the input polarizer, the Wollaston polarizer, and the retardance. Use of the ratio of the transmitted intensities normalizes fluctuations in la-

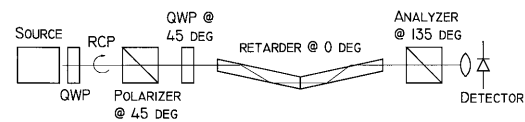


Fig. 9. Schematic of the null polarimeter with quarter-wave plate (QWP). Orientations are for fast-retarder axes or polarizer-transmission axes.

ser power as well as differences in detector gains. These intensities are measured as the input polarizer is rotated through a known range of angles, and we perform a least-squares fit to the governing equation to determine retardance. Retardance measurements with an expanded uncertainty U between 0.047° and 0.11° have been obtained with this system.¹⁸

The second method is a null technique adapted from ellipsometry,¹⁹ and the apparatus is sketched in Fig. 9. Before the retarder is inserted, the polarizer and the analyzer are crossed, and the biasing waveplate axes are aligned parallel to the polarizers. Then the retarder is inserted and oriented with its retardance axes at 45° to those of the quarter-wave plate. The polarizer is rotated until extinction occurs and the retardance is twice the angle of rotation. Retardance measurements with an expanded uncertainty less than 0.1° have been demonstrated.²⁰

Advantages of this technique include a weak dependence on the stability of the laser, on the linearity of the photodiode, and on the accuracy of the quarter-wave plates. The instrument is very sensitive to the accuracy with which the azimuthal positions of the polarizer and the analyzer can be read. An error of 1° in the orientation of the polarizer converts to an error of 2° in the measured retardance.

Finally, we developed an accurate interferometer that directly measures the phase shift between s - and p -polarized fields.²¹ The retarder is placed in one arm of a Michelson interferometer, and the input beam is linearly polarized at 45° so that the fast and the slow axes of the retarder are equally illuminated. At the output of the interferometer, a polarizing beam splitter with axes aligned to coincide with the retarder axes separates the light into two orthogonally polarized beams that are separately detected. The detected outputs follow the common sinusoidal transfer function typical of a Michelson interferometer, but the sinusoids differ by a phase bias equal to twice the actual retardance. Translating one of the mirrors at constant velocity with a piezoelectric driver scans the transfer function with time and produces the biased sinusoidal waveforms.

The phase difference between the two waveforms is accurately determined by the acquisition of the data with a computer and the application of discrete Fourier analysis. Because the two beams traverse a common path, small path changes (caused by acoustics or temperature changes, for example) affect both beams equally so the phase difference is unchanged. Retardance measurements with expanded uncertain-

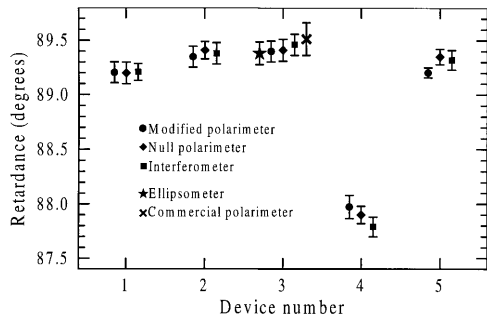


Fig. 10. Measured retardance for five prototype stable retarders.

ties between 0.08° and 0.1° have been demonstrated.²¹

Five prototype retarders were fabricated and each was measured with the three methods.^{18,20,21} Figure 10 shows the results of these comparisons. One of the retarders, designated SR3, was also measured by two other organizations with other methods.²²

7. Double-Rhomb Retarder Performance

Retardances measured for the five devices (see Fig. 10) were from 0.6° to 2.4° lower than theory predicted. TIR retardance typically depends on surface treatment,^{23,24} and we attribute this difference to the effect of moisture, as we discussed previously. Baking newly fabricated rhombs at 90°C for 1 to 2 weeks removes water adsorbed onto the surface and increases the retardance to the theoretically predicted value. The retardance of rhombs exposed to humidity for months could not be changed much by heating, however, and we suspect that diffusion and chemical bonding of water occurs for longer exposures. We now routinely bake rhombs to drive off moisture before we package them.

Figure 11 shows the spatial variation in retardance for a 2-mm diameter ($1/e^2$) beam that was normally

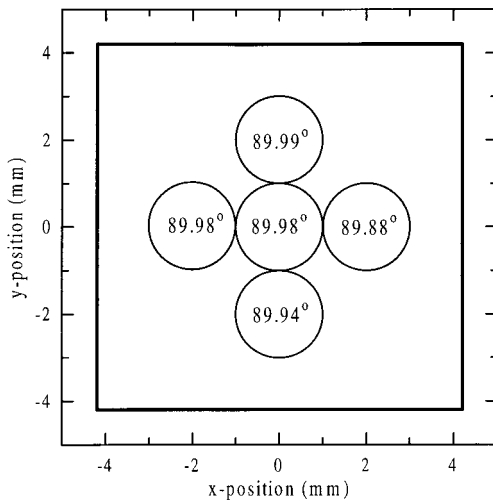


Fig. 11. Retardance across the input face of the device measured with a 2-mm-diameter beam. The thick square indicates the usable area of the device defined by the epoxy seal.

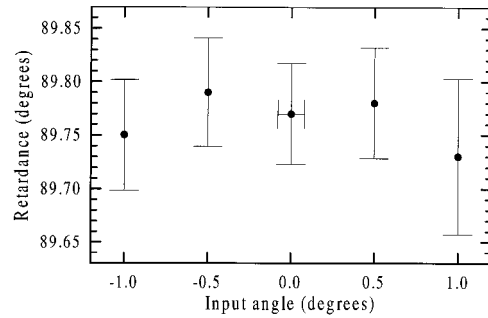


Fig. 12. Measured retardance at various input angles.

incident at several positions on the input face. Figure 12 shows the variation with input angle; for angles greater than approximately 1° , the 3-mm beam is clipped, and retardance measurements might be erroneous. We have fabricated 3-mm diameter pinholes that can be inserted into the package window to ensure that the rhomb is within $\pm 0.6^\circ$ of normal incidence. Figure 13 shows the retardance at several wavelengths. These measurements, taken with the modified polarimeter,¹⁸ demonstrate that the device is stable within $\pm 0.1^\circ$ for these operational variables.

Temperature-induced retardance changes in packaged devices are smaller than our measurement resolution if the device is allowed to equilibrate at temperatures within 10° of room temperature. The effect of changing the temperature, which should cause larger retardance changes as thermal gradients create additional differential stresses, is shown in Fig. 14. A temperature change of $0.3^\circ/\text{min}$ causes a retardance change of 0.14° . Although these thermal shocks cause acceptably small retardance changes, we recommend allowing the device to equilibrate to laboratory temperature before use.

Figure 15 shows the result of many retardance measurements of a packaged device; these measurements were made over 18 months. Between measurements we stored the device at a nominal temperature of 25°C with relative humidity between 10 and 60%. The variation in retardance is comparable with the precision of our measurements, so no change in retardance with time is discernible.

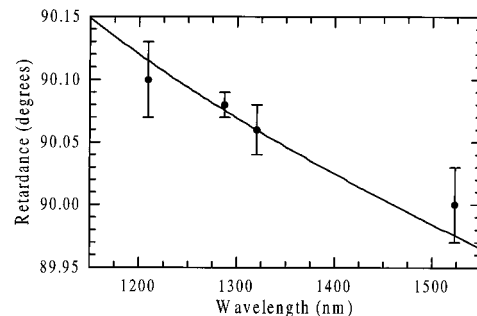


Fig. 13. Measured retardance at several wavelengths; compared with theory, the solid line is the slope expected from glass dispersion, offset to match the measured retardance at 1320 nm.

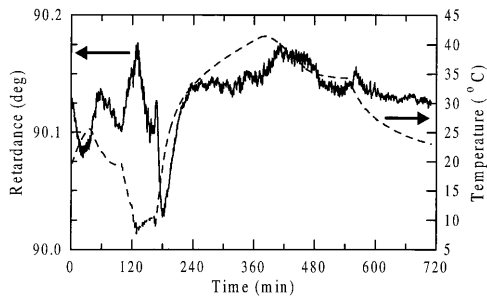


Fig. 14. Response of packaged device to thermal variations.

8. Conclusions

A linear retarder with better than $\pm 0.1^\circ$ stability has been developed and demonstrated. Use of a low stress-optic-coefficient glass provides immunity from stress and allows us to exploit a design that is highly tolerant to input angle. This immunity also mitigated retardance changes that arose from strains induced by packaging and from thermal expansion. The design is achromatic, and use at wavelengths between 400 and 2200 nm requires only a change in the center wavelength of the antireflection coating. A robust packaging design protects the device from contaminants and extends the useful lifetime of this device to 10 yr.

We developed three measurement methods and demonstrated absolute accuracy by intercomparing measurements. A polarimetric method has been adopted for the characterization and certification of future devices. NIST will provide stable linear retarders with certified retardance values through its Standard Reference Materials Program.²⁵

Appendix A

Evaluating package lifetime requires combining estimates of the amount of moisture entering the box through the adhesive and gasket seals, the effective internal humidity after water absorption by the desiccant, and the change in rhomb retardance due to humidity. We assume that the initial water vapor concentration in the box is zero, the concentration outside the box is constant, and the water concentration decreases linearly across the width of the seal (from the outside to the inside edges). Using these

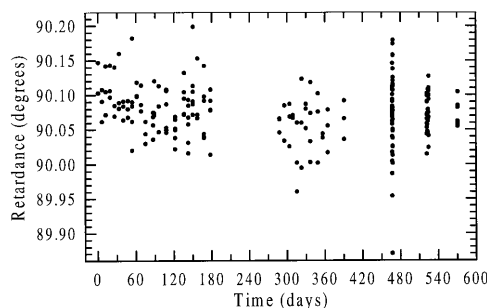


Fig. 15. Measured retardance of a packaged rhomb over a period of 18 months. After day 440, the system was modified to make numerous measurements during a single day

assumptions, Fick's first and second laws of diffusion, and Henry's law,^{26,27} we derive that the mass rate of water vapor into the box is

$$\frac{dm(t)}{dt} = \left(\frac{PA}{w}\right)_T S \times \left[\frac{RH_O - RH_I(t)}{100}\right], \quad (\text{A1})$$

where $m(t)$ is the water vapor mass (mg), A is the exposed area of the seals (cm^2), w is the seal width (mm), S is the saturation vapor pressure of water (kPa). RH_O is the constant relative humidity outside the box, $RH_I(t)$ is the inside relative humidity, and both are expressed in percentages. The water vapor permeability P of the seal material has units of $(\text{mg mm})/(\text{cm}^2 \text{ s kPa})$ and varies with temperature.²⁸ The total mass rate per unit pressure for all three seals $(PA/w)_T$ is found by summing contributions from the gasket and both optical port seals:

$$\left(\frac{PA}{w}\right)_T = \frac{P_g A}{w} \Big|_{\text{gasket}} + 2 \frac{P_w A}{w} \Big|_{\text{window}}. \quad (\text{A2})$$

Assuming $RH_I(t) \ll RH_O$, Eq. (8) becomes

$$m(t) \approx \left(\frac{PA}{w}\right)_T \frac{S \cdot RH_O \cdot t}{100}. \quad (\text{A3})$$

Our package design makes use of a 130- μm thick Teflon gasket [$P_g = 1.68 \times 10^{-8} \text{ mg mm}/(\text{cm}^2 \text{ s kPa})$ at 40 °C] (see Ref. 28), and a flexible adhesive [$P_w = 5.03 \times 10^{-6} \text{ mg mm}/(\text{cm}^2 \text{ s kPa})$ at 40 °C] for window sealing. Water vapor mass flow rate into the box is $S(PA/w)_T \approx 3.50 \times 10^{-6} \text{ mg/s}$ at 40 °C and most leakage occurs through the adhesive. We tested Eq. (A3) and our mass flow estimates by exposing packages loaded with desiccant to 90–95% relative humidity at 40 °C for 5–15 days and measuring the mass of water absorbed by the desiccant. For three tests, the mass predicted by Eq. (A3) differed from the measured mass by an average <1%, a value well within the uncertainty of our mass measurements.

Because $P > 0$ for the seals, our design includes $m_d \approx 3.5 \text{ g}$ of desiccant in the package to counter the influx of water vapor and keep humidity low. Fitting values from desiccant data tables,²⁹ we approximate the internal humidity as

$$RH_I(t) = 8.8 \times 10^{-4} \exp\left[\frac{43m(t)}{m_d}\right]. \quad (\text{A4})$$

Equation (A4) is not valid for high humidities that can saturate the desiccant, but it is valid for $RH_I(t) < 10\%$. Substituting Eqs. (A3) and (A4) into Eq. (8) and assuming that $\Delta\delta(0) = 0$, we obtain

$$\Delta\delta(t) \approx \frac{6.48 \times 10^{-12} m_d \Delta\delta_{RH}}{S \cdot RH_O \left(\frac{PA}{w}\right)_T} \times \exp\left[\frac{0.43}{m_d} S \cdot RH_O \left(\frac{PA}{w}\right)_T t - 1\right]. \quad (\text{A5})$$

Equation (A5) is valid for $t < t_{0.01}$, where

$$t_{0.01\%} = \frac{5.652m_d}{S \cdot \text{RH}_o \left(\frac{PA}{w} \right)_T}, \quad (\text{A6})$$

is the time (in seconds) during which $\text{RH}_I(t) \leq 0.01\%$ [and Eqs. (A3) and (A4) are valid].

This work was funded in part by the U.S. Navy Joint Service Research and Development Metrology Program. The development of the retarder was performed as part of a Cooperative Research and Development Agreement with Hewlett-Packard (HP) Corporation and Meadowlark Optics, Inc. We thank Mike McClendon and Paul Hernday of HP and Tom Baur and Michael Derks of Meadowlark for retardance measurements of device SR3 (see Ref. 22) and for their critical reading of this manuscript before its submission. We also acknowledge Shelley Etzel and Hervé Kienlen of NIST for experimental assistance, and David Braun of HP for ellipsometric measurements of TIR surfaces. Finally, we appreciate the contributions of two anonymous reviewers who provided several valuable comments and suggestions for improvement.

References and Notes

1. P. D. Hale and G. W. Day, "Stability of birefringent linear retarders (waveplates)," *Appl. Opt.* **27**, 5146–5153 (1988).
2. K. B. Rochford, P. A. Williams, A. H. Rose, I. G. Clarke, P. D. Hale, and G. W. Day, "Standard polarization components: progress toward an optical retardance standard," in *Polarization Analysis and Measurement II*, D. H. Goldstein and D. B. Chenault, eds., Proc. SPIE **2265**, 2–8 (1994).
3. J. M. Bennett, "A critical evaluation of rhomb-type quarter-wave retarders," *Appl. Opt.* **9**, 2123–2129 (1970).
4. N. N. Nagib and S. A. Khodier, "Optimization of a rhomb-type quarter-wave phase retarder," *Appl. Opt.* **34**, 2927–2930 (1995).
5. R. M. A. Azzam and M. M. K. Howlader, "Silicon-based polarization optics for the 1.3 and 1.55- μm communications wavelengths," *J. Lightwave Technol.* **14**, 873–878 (1996).
6. N. N. Nagib, M. S. El-Bahrawy, S. E. Demian, and S. Khodier, "Oblique incidence in total internal reflection phase retarders. II - Application," *Opt. Pura Apl.* **27**, 111–116 (1994).
7. R. J. King, "Quarter-wave retardation systems based on the Fresnel rhomb principle," *J. Sci. Instrum.* **43**, 617–622 (1966).
8. A. E. Oxley, "On apparatus for the production of circularly polarized light," *Philos. Mag.* **21**, 517–532 (1911).
9. V. A. Kizel, Y. I. Krasilov, and V. N. Shamraev, "Achromatic $\lambda/4$ device," *Opt. Spectrosc.* **17**, 248, 249 (1964).
10. SF-57, the Schott Glaswerke (Mainz, Germany) trade name for its 847238 glass, was used in our rhomb. NIST does not endorse this glass, and similar glasses produced by other manufacturers might work as well or better. The glass code (in the form xxxxyy, where xxx = $n_d - 1$, and yy = $\nu_D \times 10$) gives the refractive index and Abbé number at 587.6 nm.
11. "The stress-optical coefficients of optical glasses," Technical Note 15, 1984 (Schott Glaswerke, Mainz, Germany).
12. G. W. Day and A. H. Rose, "Faraday effect sensors: the state of the art," in *Fiber Optic and Laser Sensors*, R. P. DePaula and E. Udd, eds., Proc. SPIE **985**, 138–150 (1988).
13. The following Sellmeier equation for use in the near infrared was supplied by Schott Glass Technologies, Inc., Duryea, Pa.: $n^2 = 1 + B_1\lambda^2/(\lambda^2 - C_1) + B_2\lambda^2/(\lambda^2 - C_2) + B_3\lambda^2/(\lambda^2 - C_3)$, where λ is the wavelength (in micrometers), $B_1 = 1.816\ 513\ 71$, $B_2 = 0.428\ 893\ 6$, $B_3 = 1.071\ 862\ 78$, $C_1 = 1.437\ 041\ 98 \times 10^{-2}$, $C_2 = 5.928\ 011\ 72 \times 10^{-2}$, and $C_3 = 121.419\ 941$.
14. M. Born and E. Wolf, *Principles of Optics*, 6th ed. (Pergamon, Oxford, 1980) p. 50.
15. E. Hecht and A. Zajak, *Optics* (Addison-Wesley, Reading, Mass., 1974), pp. 301–305.
16. A. M. Mood, F. A. Graybill, and D. C. Boes, *Introduction to the Theory of Statistics* (McGraw-Hill, New York, 1974), p. 175.
17. B. N. Taylor and C. E. Kuyatt, *Guidelines for Evaluating and Expressing the Uncertainty of NIST Measurements*, NIST Technical Note 1297, 1993 (U.S. Government Printing Office, Washington, D.C.).
18. P. A. Williams, A. H. Rose, and C. M. Wang, "Rotating-polarizer polarimeter for accurate retardance measurement," *Appl. Opt.* **36**, 6466–6472 (1997).
19. H. G. Tompkins, *A User's Guide to Ellipsometry* (Academic, New York, 1993), pp. 26–30.
20. K. B. Rochford and C. M. Wang, "Uncertainty in null polarimeter measurements," IR 5055, 1996 (National Institute of Standards and Technology, Gaithersburg, Md.).
21. K. B. Rochford and C. M. Wang, "Accurate interferometric retardance measurements," *Appl. Opt.* **36**, 6473–6479 (1997).
22. Measurements were made at Hewlett-Packard, Santa Rosa Lightwave Operation (Santa Rosa, Calif.) with a commercial polarimeter and at Meadowlark Optics (Longmont, Colo.) with a filtered-source ellipsometer.
23. Lord Rayleigh, "The surface layer of polished silica and glass with further studies on optical contact," *Proc. R. Soc. London Ser. A*, **160**, 507–525 (1937).
24. R. W. Ditchburn and G. A. Orchard, "The polarization of totally reflected light," *Proc. R. Soc. London Ser. B* **67**, 608–614 (1954).
25. Standard Reference Materials Program, National Institute of Standards and Technology, Gaithersburg, Md. 20899.
26. J. Comyn, "Introduction to polymer permeability and the mathematics of diffusion," in *Polymer Permeability*, J. Comyn, ed. (Chapman and Hall, London, 1994), pp. 1–10.
27. M. Tencer, "Moisture ingress into nonhermetic enclosures and packages. A quasi-steady-state model for diffusion and attenuation of ambient humidity variations," in *Proceedings of the 44th Electronic Components and Technology Conference* (IEEE, New York, 1994), pp. 196–209.
28. S. Pauly, "Permeability and diffusion data," in *Polymer Handbook*, 3rd ed., J. Brandrup and E. H. Immergut, eds. (Wiley Interscience, New York, 1989), pp. VI:435–449.
29. UOP, Inc., "Molecular sieve water and air data sheets," Technical sheet F-43C-6, 1991 (Houston, Tex.).